

Relic density of dark matter in the NMSSM

G. Bélanger¹, F. Boudjema¹, C. Hugonie², A. Pukhov³, A. Semenov⁴

1) Laboratoire de Physique Théorique LAPTH, F-74941 Annecy-le-Vieux, France

2) Laboratoire de Physique Théorique, Univ. Paris XI, F-91405 Orsay, France

3) Skobeltsyn Inst. of Nuclear Physics, Moscow State Univ., 119992 Moscow, Russia

4) Joint Inst. for Nuclear Research, 141980 Dubna, Russia

October 17, 2018

Abstract

We present a code to compute the relic density of dark matter in the Next-to-Minimal Supersymmetric Standard Model (NMSSM). Dominant corrections to the Higgs masses are calculated with NMHDECAY as well as theoretical and collider constraints. All neutralino annihilation and coannihilation processes are then computed with an extended version of micrOMEGAs, taking into account higher order corrections to Higgs vertices. We explore the parameter space of the NMSSM and consider in particular the case of a bino LSP, of a mixed bino-higgsino LSP and of a singlino LSP. As compared to the MSSM, neutralino annihilation is often more efficient as it can take place via (additional) Higgs resonances as well as annihilation into light Higgs states. Models with a large singlino component can be compatible with WMAP constraints.

1 Introduction

In any supersymmetric (SUSY) extension of the Standard Model (SM) with conserved R-parity, the lightest SUSY particle (LSP) constitutes a good candidate for cold dark matter. Recent measurements from WMAP [1] have constrained the value for the relic density of dark matter within 10% ($.0945 < \Omega h^2 < .1287$ at 2σ). The forthcoming PLANCK experiment should reduce this interval down to 2%. It is therefore of the utmost importance to calculate the relic density as accurately as possible in any given SUSY model, in order to match this experimental accuracy. This has been done in the context of the Minimal Supersymmetric Standard Model (MSSM), with the publicly available program micrOMEGAs [2]. This code computes the relic density of the lightest neutralino LSP by evaluating the thermally averaged cross section for its annihilation as well as, when necessary, for its coannihilation with other SUSY particles. It then solves the density evolution equation numerically, without using the freeze-out approximation.

The impact of the WMAP constraints on the parameter space of the MSSM has been widely studied [3]. In the mSUGRA inspired version of the MSSM, one needs rather special conditions among parameters to have a large enough annihilation cross-section and meet the constraints of WMAP. This is because the LSP is usually a bino and the main mechanism for annihilation is into fermion pairs and requires the presence of a light slepton. Given the direct constraints on light sleptons and on light neutralinos as well as on the light Higgs mass, this possibility is valid into a small corner of parameter space. Within mSUGRA models, to satisfy the WMAP constraint one must then appeal to specific processes such as

coannihilation processes, rapid annihilation through Higgs exchange or some non negligible higgsino component of the neutralino LSP. The latter condition is satisfied in the so-called focus point region of mSUGRA models. On the other hand, in the general MSSM with no assumption on GUT scale physics and free parameters at the electroweak (EW) scale, it is much easier to satisfy the upper bound on relic density from WMAP. All models with a mixed bino/higgsino or mixed bino/wino LSP annihilate much more efficiently and this even for heavy sfermions. In fact the annihilation is so efficient that the relic density often lies below the WMAP range, thus implying some additional dark matter component. Large higgsino component of the neutralino LSP means enhanced couplings to the Z boson and to the pseudo-scalar Higgs boson A , thus favouring annihilation channels into fermion pairs. Large wino component means more efficient couplings to gauge bosons favouring annihilation channels into W pairs. Furthermore coannihilation channels with a heavier neutralino and/or chargino are also enhanced for either higgsino or wino-like LSP's. In the limit where all sfermions are heavy the important parameters that enter the computation are those of the neutralino sector $M_1, M_2, \mu, \tan\beta$ as well as the pseudo-scalar Higgs mass m_A . The trilinear couplings $A_{\tilde{f}}$ can play a role for the relic density as they influence the mass of the lightest Higgs.

It is well known, however, that the MSSM faces a naturalness problem – the so-called μ problem [4] – arising from the presence of a SUSY conserving mass term for the Higgs fields in the superpotential, $\mu\widehat{H}_u\widehat{H}_d$. The only natural values for the μ parameter are either zero or the Planck scale. The first is experimentally excluded while the second reintroduces the hierarchy problem. The Next-to-Minimal Supersymmetric Standard Model (NMSSM) [5] provides an elegant solution to the μ problem via the introduction of a gauge singlet superfield \widehat{S} in the Higgs sector. Assuming the simplest possible scale invariant form of the superpotential, which contains the dimensionless $\lambda\widehat{S}\widehat{H}_u\widehat{H}_d$ coupling, the scalar component S of the singlet acquires naturally a vacuum expectation value (vev) of the order of the SUSY breaking scale, giving rise to an effective $\mu \equiv \lambda\langle S \rangle$ of order the EW scale. The NMSSM is the simplest SUSY extension of the SM in which the EW scale originates from the SUSY breaking scale *only*. Another nice feature of the NMSSM is that the fine tuning problem originating from the non-observation of a neutral Higgs boson at LEP, is less severe than in the MSSM [6]. A possible cosmological domain wall problem [7] can be avoided by introducing suitable non-renormalizable operators [8] that do not generate dangerously large singlet tadpole diagrams [9]. In addition to the MSSM fields, the NMSSM contains an extra scalar and pseudo-scalar neutral Higgs bosons, as well as an additional neutralino, the singlino. The phenomenology of the model can be markedly different from the MSSM [10]. The upper bound on the mass of the lightest Higgs state is larger than in the MSSM, up to 180 GeV [11]. Moreover, a very light Higgs boson (as light as a few GeV) is not experimentally excluded [12]. Similarly, a very light neutralino with a large singlino component may have escaped LEP searches [13]. All these properties could impact significantly the relic density computation in the NMSSM.

Up to now there has been only a few studies of the relic density of dark matter in the NMSSM [14], although a detailed analysis of dark matter direct detection in this model was recently carried out [15]. In this paper we present a code that calculates the relic density of dark matter in the NMSSM. This code provides an interface between NMHDECAY and micrOMEGAs. The FORTRAN code NMHDECAY allows a precise calculation of the particle spectrum in the NMSSM, as well as a complete check of all the available experimental constraints from LEP [16]. The parameters are then fed into a new version micrOMEGAs extended

to the NMSSM, which calculates *all* relevant cross-sections for neutralino annihilations and coannihilations and computes the relic density.

The paper is organized as follows: we first describe the model, summarize the main features of NMHDECAY and discuss the implementation of the NMSSM into CompHEP/CalcHEP and micrOMEGAs. In section 3 we give results for typical case studies. Conclusions are given in section 4.

2 Overview of the NMSSM and NMHDECAY

Extending the calculation of the lightest neutralino relic density from the MSSM to the NMSSM, requires first to compute the neutralino as well as the Higgs boson masses and mixings in this model. To achieve this task, we used the FORTRAN program NMHDECAY [16], which conventions we will review now. We then discuss the implementation of the model into CompHEP/CalcHEP and micrOMEGAs, as well as the interface between both codes. We finally give a summary of the experimental and theoretical constraints taken into account.

2.1 General Set Up

In addition to the standard MSSM Yukawa couplings for quarks and leptons, the NMSSM superpotential contains two additional terms involving the Higgs doublet superfields, \widehat{H}_u and \widehat{H}_d , and the gauge singlet \widehat{S}

$$W = \lambda \widehat{S} \widehat{H}_u \widehat{H}_d + \frac{1}{3} \kappa \widehat{S}^3. \quad (2.1)$$

As mentioned in the introduction, the superpotential in eq. (2.1) is scale invariant, and the EW scale appears only through the soft SUSY breaking terms in $\mathcal{L}_{\text{soft}}$, which in our conventions are given by

$$\begin{aligned} -\mathcal{L}_{\text{soft}} &= m_{H_u}^2 |H_u|^2 + m_{H_d}^2 |H_d|^2 + m_S^2 |S|^2 \\ &+ (\lambda A_\lambda H_u H_d S + \frac{1}{3} \kappa A_\kappa S^3 + \text{h.c.}) \\ &- \frac{1}{2} (M_2 \lambda_2 \lambda_2 + M_1 \lambda_1 \lambda_1 + \text{h.c.}). \end{aligned} \quad (2.2)$$

We denote the Higgs vevs v_u , v_d and s such that

$$H_u^0 = v_u + \frac{H_{uR} + iH_{uI}}{\sqrt{2}}, \quad H_d^0 = v_d + \frac{H_{dR} + iH_{dI}}{\sqrt{2}}, \quad S = s + \frac{S_R + iS_I}{\sqrt{2}}. \quad (2.3)$$

One can derive three minimization conditions for the Higgs vevs and use them to re-express the soft breaking Higgs masses in terms of λ , κ , A_λ , A_κ , v_u , v_d and s . It is also convenient to define the quantities

$$\mu = \lambda s, \quad \nu = \kappa s, \quad \tan\beta = \frac{v_u}{v_d} \quad \text{and} \quad v^2 = v_u^2 + v_d^2. \quad (2.4)$$

2.2 Higgs Sector

In the basis (H_{uR}, H_{dR}, S_R) one obtains the following mass matrix for the neutral scalar Higgs states:

$$\begin{aligned}
\mathcal{M}_{S,11}^2 &= M_Z^2 \sin^2 \beta + \mu \cot \beta (A_\lambda + \nu), \\
\mathcal{M}_{S,22}^2 &= M_Z^2 \cos^2 \beta + \mu \tan \beta (A_\lambda + \nu), \\
\mathcal{M}_{S,12}^2 &= \left(\lambda^2 v^2 - \frac{M_Z^2}{2} \right) \sin 2\beta - \mu (A_\lambda + \nu), \\
\mathcal{M}_{S,33}^2 &= \frac{\lambda^2 v^2 A_\lambda \sin 2\beta}{2\mu} + \nu (A_\kappa + 4\nu), \\
\mathcal{M}_{S,13}^2 &= \lambda v (2\mu \sin \beta - (A_\lambda + 2\nu) \cos \beta), \\
\mathcal{M}_{S,23}^2 &= \lambda v (2\mu \cos \beta - (A_\lambda + 2\nu) \sin \beta).
\end{aligned} \tag{2.5}$$

After diagonalization by an orthogonal 3×3 matrix S_{ij} one obtains 3 neutral scalars h_i (ordered in mass). Similarly, in the basis (H_{uI}, H_{dI}, S_I) , the neutral pseudo-scalar mass matrix reads

$$\begin{aligned}
\mathcal{M}_{P,11}^2 &= \mu \cot \beta (A_\lambda + \nu), \\
\mathcal{M}_{P,22}^2 &= \mu \tan \beta (A_\lambda + \nu), \\
\mathcal{M}_{P,12}^2 &= \mu (A_\lambda + \nu), \\
\mathcal{M}_{P,33}^2 &= \frac{\lambda^2 v^2 \sin 2\beta}{2\mu} (A_\lambda + 4\nu) - 3A_\kappa \nu, \\
\mathcal{M}_{P,13}^2 &= \lambda v \cos \beta (A_\lambda - 2\nu), \\
\mathcal{M}_{P,23}^2 &= \lambda v \sin \beta (A_\lambda - 2\nu).
\end{aligned} \tag{2.6}$$

Eliminating the Goldstone mode by the rotation:

$$\begin{pmatrix} H_{uI} \\ H_{dI} \\ S_I \end{pmatrix} = \begin{pmatrix} \cos \beta & -\sin \beta & 0 \\ \sin \beta & \cos \beta & 0 \\ 0 & 0 & 1 \end{pmatrix} \begin{pmatrix} A \\ G \\ S_I \end{pmatrix} \tag{2.7}$$

the 2×2 pseudo-scalar mass matrix in the basis (A, S_I) has the following matrix elements

$$\begin{aligned}
\mathcal{M}'_{P,11}{}^2 &= \frac{2\mu}{\sin 2\beta} (A_\lambda + \nu), \\
\mathcal{M}'_{P,22}{}^2 &= \frac{\lambda^2 v^2 \sin 2\beta}{2\mu} (A_\lambda + 4\nu) - 3A_\kappa \nu, \\
\mathcal{M}'_{P,12}{}^2 &= \lambda v (A_\lambda - 2\nu).
\end{aligned} \tag{2.8}$$

It can be diagonalized by an orthogonal 2×2 matrix P'_{ij} , yielding 2 neutral pseudo-scalars a_i (ordered in mass). Finally, the charged Higgs mass is given by

$$m_{h^\pm}^2 = \frac{2\mu}{\sin 2\beta} (A_\lambda + \nu) + M_W^2 - \lambda^2 v^2. \tag{2.9}$$

In the MSSM limit ($\lambda \rightarrow 0$, μ fixed) one obtains 2 quasi pure singlet states with masses

$$m_S^2 = \nu(A_\kappa + 4\nu), \quad m_P^2 = -3A_\kappa\nu. \quad (2.10)$$

In the doublet sector, one can define

$$m_A^2 = \mathcal{M}_{P,11}'^2 = \frac{2\mu}{\sin 2\beta} (A_\lambda + \nu). \quad (2.11)$$

In the limit $m_A \gg M_Z$, the masses of one scalar, one pseudo-scalar and the charged Higgs states are $\approx m_A$. The mass of the lightest scalar Higgs is bounded by

$$m_{h_1}^2 \leq M_Z^2 \cos^2 2\beta + \lambda^2 v^2 \sin^2 2\beta. \quad (2.12)$$

In order to calculate the relic density, one needs the Feynman rules for triple Higgs interactions, in case the LSP annihilates into a Higgs pair through s-channel Higgs boson exchange. We give here the coupling of a non-singlet scalar h_i to 2 quasi pure singlet pseudo-scalars P :

$$g_{h_i PP} = \sqrt{2}\lambda^2 v (S_{i1} \sin\beta + S_{i2} \cos\beta) + \sqrt{2}\lambda\kappa v (S_{i2} \sin\beta + S_{i1} \cos\beta). \quad (2.13)$$

The complete formulae for the triple Higgs interactions can be found in ref. [16].

2.3 Neutralino Sector

In the basis $(\tilde{B}, \tilde{W}, \tilde{H}_u, \tilde{H}_d, \tilde{S})$ the 5×5 neutralino mass matrix reads

$$\mathcal{M}_{\tilde{\chi}^0} = \begin{pmatrix} M_1 & 0 & M_Z \sin\theta_W \sin\beta & -M_Z \sin\theta_W \cos\beta & 0 \\ 0 & M_2 & -M_Z \cos\theta_W \sin\beta & M_Z \cos\theta_W \cos\beta & 0 \\ M_Z \sin\theta_W \sin\beta & -M_Z \cos\theta_W \sin\beta & 0 & -\mu & -\lambda v \cos\beta \\ -M_Z \sin\theta_W \cos\beta & M_Z \cos\theta_W \cos\beta & -\mu & 0 & -\lambda v \sin\beta \\ 0 & 0 & -\lambda v \cos\beta & -\lambda v \sin\beta & 2\nu \end{pmatrix}. \quad (2.14)$$

This matrix is diagonalized by a unitary matrix, N . The lightest neutralino LSP can then be decomposed as

$$\tilde{\chi}_1^0 = N_{11}\tilde{B} + N_{12}\tilde{W} + N_{13}\tilde{H}_u + N_{14}\tilde{H}_d + N_{15}\tilde{S}. \quad (2.15)$$

Further, we shall talk about the bino, higgsino and singlino fractions of the LSP, which we define as N_{11}^2 , $N_{13}^2 + N_{14}^2$ and N_{15}^2 respectively.

In the limit $\lambda \rightarrow 0$, the singlino is a quasi pure state with mass

$$m_{\tilde{S}} = 2\nu. \quad (2.16)$$

For the relic density calculation, the coupling of the LSP to the Z boson is relevant. This coupling depends only on the higgsino components of the LSP and is proportional to $N_{13}^2 - N_{14}^2$. The couplings of the LSP to the scalar and pseudo-scalar Higgs states will enter the computation of LSP annihilation through a Higgs resonance or t-channel annihilation into Higgs pairs. The Feynman rule for the LSP-scalar-scalar vertex reads

$$g_{\tilde{\chi}_1^0 \tilde{\chi}_1^0 h_i} = g(N_{12} - N_{11} \tan\theta_W)(S_{i1}N_{13} - S_{i2}N_{14}) + \sqrt{2}\lambda N_{15}(S_{i1}N_{14} + S_{i2}N_{13}) + \sqrt{2}S_{i3}(\lambda N_{13}N_{14} - \kappa N_{15}^2). \quad (2.17)$$

The first term is equivalent to the $\tilde{\chi}_1^0 \tilde{\chi}_1^0 h$ coupling in the MSSM by replacing $S_{11} = S_{22} = \cos\alpha$ and $S_{12} = -S_{21} = \sin\alpha$ while the last two terms are specific of the NMSSM. The second term is proportionnal to the the singlino component of the LSP while the last one is proportionnal to the singlet component of the scalar Higgs. The latter involves either the higgsino component of the LSP or its singlino component. When the LSP has a very small singlino component, then as in the MSSM, coupling to the scalars requires a mixed bino/higgsino LSP. Typically in models with a very light scalar Higgs, this one has an important singlet component and the coupling to the LSP is given by the last term in eq. (2.17). Similarly, the LSP coupling to a pseudo-scalar reads

$$ig_{\tilde{\chi}_1^0 \tilde{\chi}_1^0 a_i} = g(N_{12} - N_{11} \tan\theta_W)(P_{i1}N_{13} - P_{i2}N_{14}) - \sqrt{2}\lambda N_{15}(P_{i1}N_{14} + P_{i2}N_{13}) - \sqrt{2}P_{i3}(\lambda N_{13}N_{14} - \kappa N_{15}^2). \quad (2.18)$$

2.4 Radiative Corrections

Similarly to the MSSM, radiative corrections to the Higgs masses in the NMSSM can be relatively large [11]. As said earlier, in order to calculate the Higgs spectrum, we used the program NMHDECAY [16]. Let us review now the accuracy with which radiative corrections are computed for the Higgs sector in this program.

First, we assume that the Yukawa couplings and the soft terms are defined at the SUSY breaking scale $Q = M_{\text{SUSY}}$, corresponding to an average of the squark masses. Quantum fluctuations at higher scales are assumed to be integrated out through the standard renormalization group evolution of the parameters from a fundamental scale like M_{GUT} down to the scale Q . The effective Lagrangian at the scale Q can be assumed to be of the standard SUSY form plus soft terms. The full effective action then reads

$$\Gamma_{\text{eff}} = \sum_i Z_i D_\mu H_i D^\mu H_i - V_{\text{eff}}(H_i). \quad (2.19)$$

It is obtained from the effective Lagrangian at the scale Q by adding all quantum effects arising from fluctuations at scales $\lesssim Q$. (Here, H_i denotes all the Higgs fields, H_u , H_d and S .) These quantum effects can be classified according to powers of the various couplings, and powers of potentially large logarithms.

Let us start with the corrections to the effective potential. It is somehow more convenient to classify the corrections to the (lightest) scalar Higgs mass, which is essentially the second derivative of the effective potential. At tree level, one can rewrite eq. (2.12) as

$$m_{h_1}^2 \sim (g^2 + \lambda^2)v^2 \quad (2.20)$$

where g denotes the weak gauge couplings (we do not distinguish between large and small $\tan\beta$ here).

The dominant one loop corrections to $m_{h_1}^2$ originate from top, stop, bottom and sbottom loops. The corresponding corrections $\delta m_{h_1}^2$ to $m_{h_1}^2$ are of order

$$\begin{aligned} \delta_t m_{h_1}^2 &\sim h_t^4 v^2 \ln(Q^2/m_t^2) \quad , \quad \delta_{\bar{t}} m_{h_1}^2 \sim h_{\bar{t}}^4 v^2 \quad , \\ \delta_b m_{h_1}^2 &\sim h_b^4 v^2 \ln(Q^2/m_b^2) \quad , \quad \delta_{\bar{b}} m_{h_1}^2 \sim h_{\bar{b}}^4 v^2 \quad . \end{aligned} \quad (2.21)$$

These contributions to the effective potential are computed exactly, without expanding in large logarithms or squark mass splittings. We also take into account the one loop pure weak (leading log) contributions of the order $g^4 \ln(Q^2/M_Z^2)$.

The dominant two loop corrections to the effective potential are of the form

$$\delta_2 m_{h_1}^2 \sim (h_t^6 + h_t^4 \alpha_s) v^2 \ln^2(Q^2/m_t^2) . \quad (2.22)$$

Here, only the leading (double) logarithms are included, i.e. we neglect single logs as well as terms involving bottom and sbottom loops, proportional to powers of h_b .

Next, we review the contributions to the wave function normalization constants Z_i in eq. (2.19). If evaluated for external momenta of $\mathcal{O}(m_t)$ (the order of the Higgs masses), top and bottom quark loops yield contributions to Z_i of the form

$$Z_u \sim 1 + h_t^2 \ln(Q^2/m_t^2) , \quad Z_d \sim 1 + h_b^2 \ln(Q^2/m_t^2) . \quad (2.23)$$

After rescaling the Higgs fields so that their kinetic energies are canonically normalized, these effects generate contributions $\delta_Z m_{h_1}^2$ which take the form

$$\delta_Z m_{h_1}^2 \sim (g^2 + \lambda^2)(h_t^2 + h_b^2) \ln(Q^2/m_t^2) . \quad (2.24)$$

Once the Higgs mass matrices are diagonalized, one may find eigenstates with masses m_H substantially larger than m_t . The Z factors are then evaluated at external momenta of $\mathcal{O}(m_H)$, i.e. at the pole of the propagators. Hence for $m_H \gg m_t$ the logarithms $\ln(Q^2/m_t^2)$ in eq. (2.23) is replaced by $\ln(Q^2/m_H^2)$, with coefficients depending on Higgs mixing matrices.

2.5 Implementation into CompHEP/CalcHEP and micrOMEGAs

The power of micrOMEGAs [2] is that given a set of parameters in the MSSM or in the NMSSM it first isolates the LSP before generating, for any given situation including those where coannihilations occur, all the necessary matrix elements of all relevant processes. Moreover an automatic procedure for looking for s-channel poles is incorporated into the program such that a more precise integration routine can be used in the event one is close to a pole. This way, any kind of annihilation or coannihilation that may be imagined is readily dealt with. This is possible thanks to the high level of automation based on the computation of cross sections through CompHEP/CalcHEP [17]. Moreover an important advantage is the ease with which a complicated model such as the NMSSM with its many fields and parameters, and therefore an extremely long list of defining Feynman rules, can be implemented in this package [18]. The gruesome task of having to code all possible vertices that appear in the NMSSM in order to generate the matrix elements is taken care of by yet another automatic procedure that only requires to define the Lagrangian in a very compact form, through multiplets and superfields. This step is performed by LANHEP [19], a program that generates the complete set of particles and vertices once given a Lagrangian [20]. The modification of micrOMEGAs to go from the MSSM to the NMSSM is done essentially through a modification of the model file through LANHEP.

One drawback, though, is that CompHEP/CalcHEP only deals with tree-level matrix elements while for the NMSSM, some parameters, especially in the Higgs sector (notably the lightest Higgs mass and coupling to $b\bar{b}$) receive important radiative corrections. For the code to be of any use, these important radiative corrections need to be taken into account. They

are introduced in a gauge invariant and consistent way through an effective Lagrangian approach. For the case at hand, to parametrize the radiative corrections to the Higgs masses and couplings, we write a general dimension four CP conserving effective scalar potential that involves the two Higgs doublets H_u , H_d and the singlet S as

$$\begin{aligned}
V_{\text{rad}} = & \lambda_1(H_u H_u^*)^2/2 + \lambda_2(H_d H_d^*)^2/2 + \lambda_3(H_u H_u^*)(H_d H_d^*) \\
& + \lambda_4(\epsilon H_u H_d)(\epsilon H_u^* H_d^*) + \lambda_5((\epsilon H_u H_d)^2 + (\epsilon H_u^* H_d^*)^2)/2 \\
& + \lambda_1^s(H_u H_u^*)SS^* + \lambda_2^s(H_d H_d^*)SS^* + \lambda_s^s(SS^*)^2/2 \\
& + \lambda_5^s((\epsilon H_u H_d)S^2 + (\epsilon H_u^* H_d^*)S^{*2})/2 + \lambda_p^s(S^4 + S^{*4}). \tag{2.25}
\end{aligned}$$

With this effective potential, corrections to both the scalar/pseudo-scalar masses and the trilinear and the quartic Higgs vertices can be expressed in terms of the ten λ 's. The Higgs mass matrices eqs. (2.5,2.6) can be rewritten as

$$\begin{aligned}
\mathcal{M}_{S,11}^2 & \rightarrow \mathcal{M}_{S,11}^2 + 2\lambda_1 v^2 \sin^2\beta - \frac{\lambda_5^s}{2} s^2 \cot\beta, \\
\mathcal{M}_{S,22}^2 & \rightarrow \mathcal{M}_{S,22}^2 + 2\lambda_2 v^2 \cos^2\beta - \frac{\lambda_5^s}{2} s^2 \tan\beta, \\
\mathcal{M}_{S,12}^2 & \rightarrow \mathcal{M}_{S,12}^2 + (\lambda_3 + \lambda_4 + \lambda_5) v^2 \sin 2\beta + \frac{\lambda_5^s}{2} s^2, \\
\mathcal{M}_{S,33}^2 & \rightarrow \mathcal{M}_{S,33}^2 + 2(\lambda_s^s + 4\lambda_p^s) s^2, \\
\mathcal{M}_{S,13}^2 & \rightarrow \mathcal{M}_{S,13}^2 + 2\lambda_1^s v s \sin\beta + \lambda_5^s v s \cos\beta, \\
\mathcal{M}_{S,23}^2 & \rightarrow \mathcal{M}_{S,23}^2 + 2\lambda_2^s v s \cos\beta + \lambda_5^s v s \sin\beta \tag{2.26}
\end{aligned}$$

and

$$\begin{aligned}
\mathcal{M}_{P,11}^2 & \rightarrow \mathcal{M}_{P,11}^2 - 2\lambda_5 v^2 \cos^2\beta - \frac{\lambda_5^s}{2} s^2 \cot\beta, \\
\mathcal{M}_{P,22}^2 & \rightarrow \mathcal{M}_{P,22}^2 - 2\lambda_5 v^2 \sin^2\beta - \frac{\lambda_5^s}{2} s^2 \tan\beta, \\
\mathcal{M}_{P,12}^2 & \rightarrow \mathcal{M}_{P,12}^2 - \lambda_5 v^2 \sin 2\beta, \tag{2.27} \\
\mathcal{M}_{P,33}^2 & \rightarrow \mathcal{M}_{P,33}^2 - \lambda_5^s v^2 \sin 2\beta - 16\lambda_p^s s^2, \\
\mathcal{M}_{P,13}^2 & \rightarrow \mathcal{M}_{P,13}^2 - \lambda_5^s v s \cos\beta, \\
\mathcal{M}_{P,23}^2 & \rightarrow \mathcal{M}_{P,23}^2 - \lambda_5^s v s \sin\beta. \tag{2.28}
\end{aligned}$$

Finally, the charged Higgs mass eq. (2.9) can be rewritten as

$$m_{h^\pm}^2 \rightarrow m_{h^+}^2 - (\lambda_4 + \lambda_5) v^2 + \frac{\lambda_5^s s^2}{\sin 2\beta}. \tag{2.29}$$

Starting from the results for the corrected Higgs masses and mixing angles provided by NMHDECAY, we then solve for the λ 's. Having extracted these parameters LANHEP readily derives the corresponding scalar trilinear and quartic Higgs vertices. This is an extension of the procedure that was shown in detail in [21]. In the present implementation the full corrections from NMHDECAY to the Higgs masses are included. Consequently the Higgs self-couplings are effectively corrected at the same leading order. As concerns these self-couplings, the results differ somehow from those one would obtain from NMHDECAY. This is

due to the fact that, in NMHDECAY, only the one loop leading logarithms coming from third generation quarks/squarks loops are taken into account in the Higgs self couplings. This said the vertex which receives the largest correction, that is the one involving the lightest scalar $h_1 h_1 h_1$, does not contribute significantly to neutralino pair annihilation. On the other hand, as we will see next, the $h_2 a_1 a_1$ vertex often enters processes of neutralino annihilation. For these vertices higher order corrections typically do not exceed a few percent when expressed in terms of corrected masses.

2.6 Parameter Space Handling

At the EW scale, the free parameters in the Higgs sector are (at tree level): λ , κ , $m_{H_u}^2$, $m_{H_d}^2$, m_S^2 , A_λ and A_κ . Using the three minimization conditions of the Higgs potential, one can eliminate the soft Higgs masses in favour of M_Z , $\tan\beta$ and $\mu = \lambda s$. We thus consider as independent parameters the following set of variables

$$\lambda, \kappa, \tan\beta, \mu, A_\lambda, A_\kappa. \quad (2.30)$$

The soft terms in the squark and slepton sector (which enter the radiative corrections in the Higgs sector) are also fixed at the EW scale. Since the gaugino soft masses M_1 and M_2 enter the neutralino mass matrix, we will keep them as free parameters in our analysis.

We set all these parameters in the program NMHDECAY [16]. For each point in the parameter space, the program NMHDECAY first checks the absence of Landau singularities for λ , κ , h_t and h_b below the GUT scale. For $m_t^{\text{pole}} = 175\text{GeV}$, this translates into $\lambda < .75$, $\kappa < .65$, and $1.7 < \tan\beta < 54$. NMHDECAY also checks the absence of an unphysical global minimum of the scalar potential with vanishing Higgs vevs.

NMHDECAY then computes scalar, pseudo-scalar and charged Higgs masses and mixings, taking into account one and two loop radiative corrections as mentioned in section 2.4, as well as chargino and neutralino masses and mixings. Finally, all available experimental constraints from LEP are checked:

- 1) In the neutralino sector, we check that the lightest neutralino does not contribute too much to the invisible Z width ($\Gamma(Z \rightarrow \tilde{\chi}_1^0 \tilde{\chi}_1^0) < 1.76$ MeV if $m_{\tilde{\chi}_1^0} < M_Z/2$, and that $\sigma(e^+e^- \rightarrow \tilde{\chi}_1^0 \tilde{\chi}_i^0) < 10^{-2}$ pb if $m_{\tilde{\chi}_1^0} + m_{\tilde{\chi}_i^0} < 209$ GeV ($i > 1$) and $\sigma(e^+e^- \rightarrow \tilde{\chi}_i^0 \tilde{\chi}_j^0) < 10^{-1}$ pb if $m_{\tilde{\chi}_i^0} + m_{\tilde{\chi}_j^0} < 209$ GeV ($i, j > 1$). In the chargino sector, we check that the lightest chargino is not too light ($m_{\tilde{\chi}_1^\pm} < 103.5$ GeV).
- 2) In the charged Higgs sector, we impose $m_{h^\pm} > 78.6$ GeV.
- 3) In the neutral Higgs sector, we check the constraints on the production rates (reduced couplings) \times branching ratios versus the masses, for all of the CP-even states h and CP-odd states a , in all the channels studied at LEP (cf ref. [16] for details).

For points which violate either a theoretical constraint (Landau Pole or unphysical global minimum) or an experimental constraint, a warning is issued by NMHDECAY. The Higgs masses and mixings calculated in NMHDECAY are then fed into micrOMEGAs. The input parameters of the NMSSM needed by micrOMEGAs are listed in table 1, while the input parameters of the standard model are specified in ref. [2]. We assume that the masses of the first two generations of sfermions are equal. micrOMEGAs recomputes the masses of charginos, neutralinos and sfermions at tree-level. In the present version the soft terms for sfermions are used and masses and mixings are computed at tree-level. It is straightforward

to replace this with some external program (such as NMHDECAY) that calculates all masses for SUSY particles, as was done in the case of the MSSM. `micrOMEGAs` then calculates the LSP relic density, taking into account all possible annihilation and coannihilation diagrams. For triple Higgs vertices, the main corrections are included as outlined in section 2.5. For Higgs couplings to quarks, leading QCD corrections are taken into account using the running quark masses.

name	comment	name	comment
hL	λ	Mli, i=2,3	masses of left sleptons
hK	κ	Mri, i=2,3	masses of right sleptons
tb	$\tan\beta$	Mqi, i=2,3	masses of left squarks
mu	μ	Mui, i=2,3	masses of right u-squarks
hLs	A_λ	Mdi, i=2,3	masses of right d-squarks
hKs	A_κ		
MG1	M_1	Al	$\tilde{\tau}$ trilinear coupling
MG2	M_2	Ab	\tilde{b} trilinear coupling
MG3	M_3	At	\tilde{t} trilinear coupling

Table 1: Input parameters for `micrOMEGAs_nmssm`.

3 Results

In this section, we discuss constraints on the parameter space of the NMSSM originating from the WMAP results on dark matter relic density. To avoid having to deal with a large number of parameters, we assume very heavy sfermions ($m_{\tilde{f}} = 1$ TeV) and fix the trilinear sfermion mixing $A_{\tilde{f}} = 1.5$ TeV. Thus annihilation into fermion pairs through t-channel sfermion exchange and coannihilation with sfermions are suppressed. In the gaugino sector, we assume universality at the GUT scale, which at the EW scale corresponds to $M_2 = 2M_1$ and $M_3 = 3.3M_2$. The parameters of our model are thus $\lambda, \kappa, \mu, \tan\beta, A_\lambda, A_\kappa$ and M_2 . These parameters are free parameters at the EW scale. For the SM parameters, we assume $\alpha_s = 0.118$, $m_t^{\text{pole}} = 175$ GeV and $m_b(m_b) = 4.24$ GeV.

We concentrate on models which can differ markedly from the MSSM predictions, in particular models with $\tan\beta \leq 5$ for which annihilation through a Higgs resonance is marginal in the MSSM. First we study the behaviour of Ωh^2 as a function of μ and M_2 . Then, picking values for μ, M_2 corresponding to typical cases, we present contour plots in the λ, κ plane, where the difference between the MSSM (which we recover at small λ) and the NMSSM appears explicitly. The parameters A_λ, A_κ are also critical as they affect the masses of the Higgs states and therefore the regions of parameter space where rapid annihilation through a Higgs resonance can take place. Finally, we present some choices of parameters for which the LSP is mainly singlino and the relic density still agrees with the WMAP constraints.

3.1 MSSM-like case: dependence in $\mu - M_2$

To give an overview of the behaviour of the relic density in the μ, M_2 plane, in fig. 1 we consider a model with $\lambda = 0.1, \kappa = 0.1, \tan\beta = 5, A_\lambda = 500 \text{ GeV}, A_\kappa = 0$. For this choice of parameters the singlino component of the LSP is small so that apart from the Higgs sector and the heavy neutralinos, the model is MSSM-like. Since the parameters are not specially tuned to encounter Higgs resonances one expects the predictions for the relic density to be rather similar to the MSSM. The LEP exclusion region arises from the limit on chargino pair production. For this choice of parameters the LEP limits on the Higgs sector does not play a role. Compatibility with WMAP is found in two different regions of the μ, M_2 plane, similar to the ones obtained in the MSSM at small to intermediate values of $\tan\beta$.

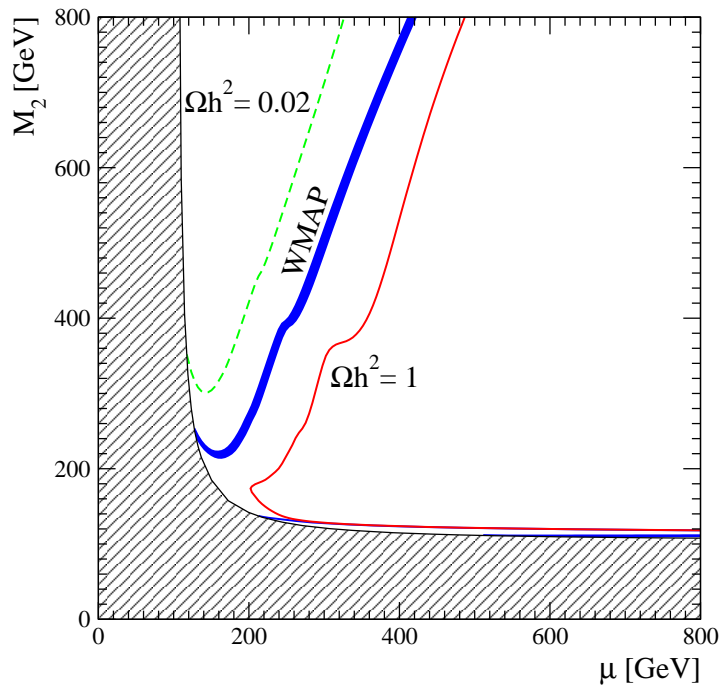


Figure 1: Contour plots for $\Omega h^2 = 0.02$, $0.0945 < \Omega h^2 < 0.1287$ (WMAP constraint) and $\Omega h^2 = 1$ in the μ, M_2 plane for $\lambda = 0.1, \kappa = 0.1, \tan\beta = 5, A_\lambda = 500 \text{ GeV}$ and $A_\kappa = 0$. The hatched region is excluded by LEP constraints on charginos.

The first region corresponds to a very thin band with $\mu \gg M_2$, just at the boundary of the region ruled out by the LEP constraint on charginos. Although in this case the LSP is mostly a bino, efficient annihilation is possible via s-channel scalar Higgs (h_1) exchange. However some fine-tuning is required to adjust the mass of the LSP to half the mass of h_1 . We will come back to this bino LSP scenario in section 3.2

The second region is a band where $\mu \gtrsim M_1 = M_2/2$. There, the LSP is mostly bino with just enough higgsino component to annihilate efficiently into gauge boson pairs (WW, ZZ). This is essentially s-channel annihilation via scalar Higgs or Z exchange as well as t-channel chargino/neutralino exchange. The higgsino fraction necessary to obtain $\Omega h^2 \approx 0.1$ increases with the LSP mass, from 25% when $m_{\tilde{\chi}_1^0} = 140 \text{ GeV}$ to 50% when $m_{\tilde{\chi}_1^0} = 400 \text{ GeV}$. When μ

and M_2 are large enough so that $m_{\tilde{\chi}_1^0} > m_t$, annihilation into top quark pairs also contributes significantly. The onset of the top pair annihilation shows up as a kink on the WMAP allowed band. Finally, note that for $M_2 < 200$ GeV and $\mu \approx M_2$ the relic density is above WMAP. This is because on the one hand the LSP bino component is large and on the other hand the gauge boson pair channel is not kinematically available. In section 3.4 we will study this mixed bino/higgsino case in more details.

To the left of the last region, the LSP is mainly higgsino and annihilation into gauge boson pairs is efficient. For a higgsino LSP, coannihilation processes with charginos and neutralinos also contribute significantly. Therefore, the relic density is very small in this region. However, increasing the singlino content of the LSP may rise the relic density inside the WMAP allowed range. We will come back to this possibility in section 3.5.

To the right of the WMAP allowed band, the LSP bino component is large while no Higgs state has the appropriate mass for a s-channel resonance (recall that we assume heavy sfermions, so annihilation to fermions through t-channel sfermion exchange is suppressed). Hence, for our choice of parameters, the relic density is large in this region of the μ, M_2 plane. However, for different choices of parameters, one may find areas where s-channel Higgs resonances bring the relic density down in this region. We will present such scenarios in section 3.3.

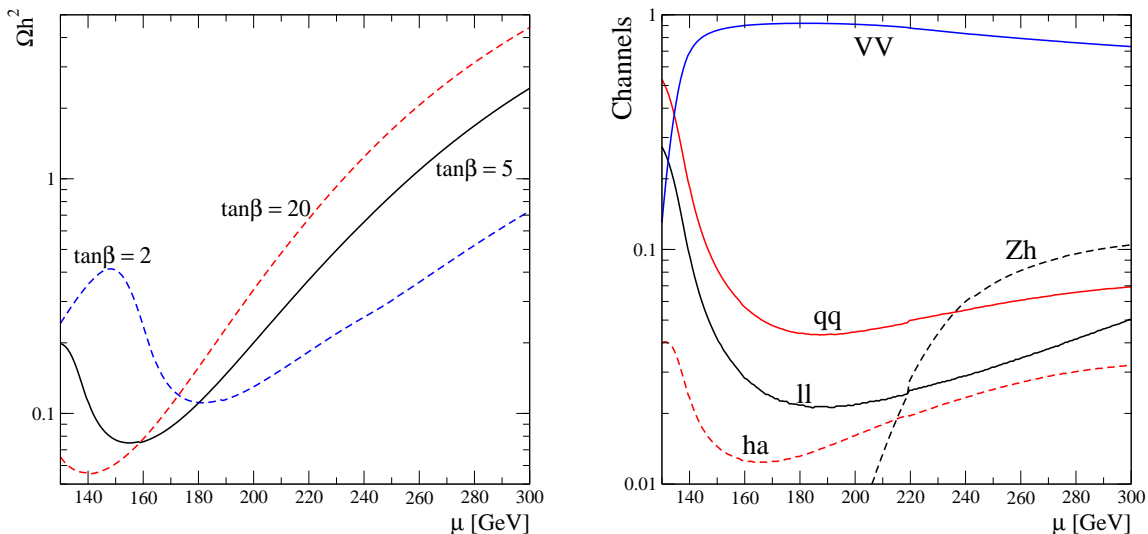


Figure 2: a) Ωh^2 as a function of μ for $\lambda = 0.1, \kappa = 0.1, A_\lambda = 500$ GeV, $A_\kappa = 0, M_2 = 230$ GeV, $\tan\beta = 5$ (full) and $\tan\beta = 2, 20$ (dash). b) Relative contribution of the main annihilation channels for the case $\tan\beta = 5$. Here VV includes both WW and ZZ channels and qq is the sum over all the quarks.

To illustrate more precisely the main mechanisms at work for the LSP annihilation, we fix $M_2 = 230$ GeV and plot the relic density as a function of μ in fig. 2. The relative contributions of the most important channels are also displayed. At small values of μ , the LSP mass is below M_W and the main annihilation channel is into $q\bar{q}$ pairs through Z exchange. The $b\bar{b}$ channel is enhanced as it receives an additional contribution from h_1 exchange. As μ increases, so does the LSP mass. Annihilation into gauge boson pairs rises

sharply and the relic density drops. The WW mode is typically 4 times larger than the ZZ mode. For larger μ , the LSP becomes less higgsino and the relic density increases (recall that the LSP coupling to gauge bosons depends only on its higgsino components). A subdominant contribution arises from the $h_1 a_1$ channel. This mode is kinematically accessible over the whole region probed since the scalar mass is $m_{h_1} \approx 118$ GeV, the pseudo-scalar mass is $m_{a_1} \approx 20$ GeV and the LSP mass range is $75 < m_{\tilde{\chi}_1^0} < 109$ GeV. For $\mu > 200$ GeV, the Zh_1 annihilation channel becomes kinematically accessible. While this channel accounts for up to 10% of all annihilations, this contribution is not sufficient to bring the relic density within the WMAP range.

In fig. 2a we also show the relic density for $\tan\beta = 2, 20$. Changing $\tan\beta$ affects the LSP mass as well as its bino/higgsino fraction, thus having a large impact on the relic density. First, the LSP mass increases with $\tan\beta$. This explains why at small μ (where one can be below the WW threshold) the relic density is smaller at large $\tan\beta$. On the other hand, the bino component of the LSP increases with $\tan\beta$. Hence, for $\mu \gtrsim 180$ GeV (where the WW channel is kinematically open for all values of $\tan\beta$) annihilation is more efficient at low values of $\tan\beta$.

3.2 Bino LSP, annihilation through h_1

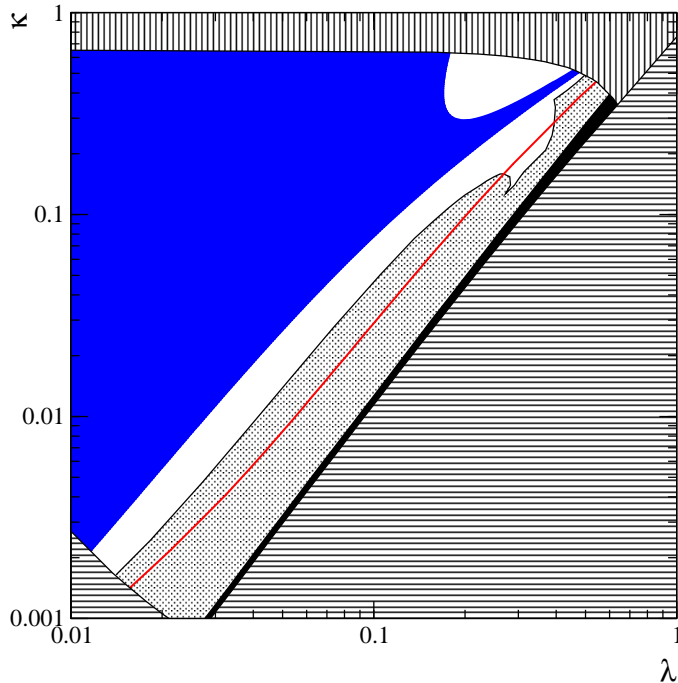


Figure 3: Region in the λ, κ plane for which $0.0945 < \Omega h^2 < 0.1287$ (blue) for $\mu = 700$ GeV, $M_2 = 111$ GeV, $A_\lambda = 500$ GeV, $A_\kappa = 0$, $\tan\beta = 5$ and contour curve for $\Omega h^2 = 1$ (red). The theoretically/experimentally excluded regions are also displayed: LEP Higgs exclusion (grey), Landau pole (vertical lines), negative Higgs mass squared (horizontal lines) and non-physical global minima of the scalar potential (black).

If $\mu \gg M_2$, the LSP is almost a pure bino (more than 99%), and the relic density is large (t-channel sfermion exchange is suppressed for heavy sfermions and annihilation through s-channel Z requires some higgsino component) unless annihilation proceeds through a s-channel Higgs resonance. In this case, the relic density is very sensitive to the mass difference, $m_{h_1} - 2m_{\tilde{\chi}_1^0}$ [22, 23]. For $\lambda = \kappa = 0.1$, $\tan\beta = 5$, $A_\lambda = 500$ GeV, $A_\kappa = 0$, $\mu = 700$ GeV, and $M_2 = 111$ GeV (corresponding to the first WMAP allowed region in fig. 1) we have such a h_1 resonance. We first examine the dependence of Ωh^2 on the specific NMSSM parameters λ, κ in fig. 3. In this plane, small values of κ/λ are excluded by either LEP Higgs searches, an unphysical global minimum of the scalar potential or a negative mass squared for the lightest pseudo-scalar. Large values of κ give rise to a Landau pole and are also excluded. Most of the remaining parameter space is allowed by the WMAP constraints.

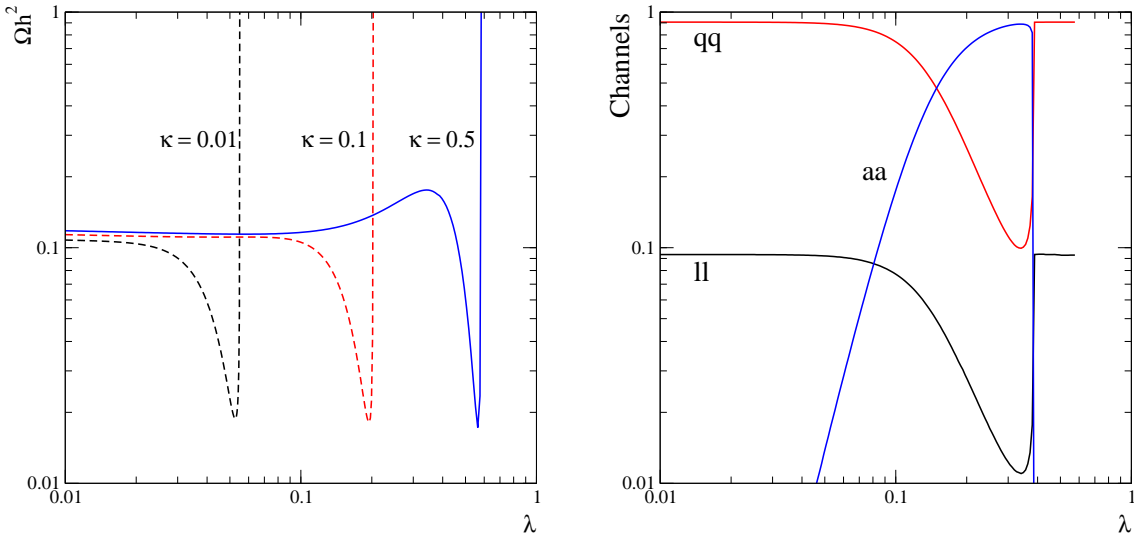


Figure 4: a) Ωh^2 vs λ for $\mu = 700$ GeV, $M_2 = 111$ GeV, $\kappa = 0.01, 0.1, 0.5$, $A_\lambda = 500$ GeV, $A_\kappa = 0$ and $\tan\beta = 5$. b) Relative contribution of the main annihilation channels for the case $\kappa = 0.5$.

Next we fix κ and study the variations of Ωh^2 as a function of λ in fig. 4. We also display the relative contributions of the most important channels. For $\lambda = 0.01, \kappa = 0.1$, one has $m_{\tilde{\chi}_1^0} = 54$ GeV and $m_{h_1} = 117$ GeV so that $m_{h_1} - 2m_{\tilde{\chi}_1^0} = 9$ GeV. A tiny higgsino fraction ($\lesssim 10^{-5}$) is then sufficient to give the right amount of relic density ($\Omega h^2 = 0.113$). As λ increases, m_{h_1} decreases whereas $m_{\tilde{\chi}_1^0}$ remains almost constant. Hence the mass difference decreases and the relic density drops sharply. When the LSP mass is above the light Higgs resonance there is no efficient mechanism for LSP annihilation and the value of the relic density shoots up. Note that for $\kappa = 0.5$, Ωh^2 first increases with λ before dropping, due to a small increase of the h_1 mass with λ , and so of $m_{h_1} - 2m_{\tilde{\chi}_1^0}$. This corresponds to the small region at large κ where the relic density is above the WMAP limit in fig. 3.

The main annihilation channels are characteristics of the dominant decay modes of the h_1 . For small λ , the main channels are $\tilde{\chi}_1^0 \tilde{\chi}_1^0 \rightarrow b\bar{b}$ and $\tau\bar{\tau}$. When λ increases, the channel $\tilde{\chi}_1^0 \tilde{\chi}_1^0 \rightarrow a_1 a_1$ becomes dominant, a_1 being a light quasi pure singlet pseudo-scalar. This is due to the fact that the $h_1 a_1 a_1$ coupling increases with λ , as can be seen from eq. (2.13).

On the other hand, the a_1 mass also increases with λ (cf. $\mathcal{M}_{P,33}$ in eq. (2.6) with $A_\kappa = 0$), so that for $\lambda \gtrsim 0.4$ this channel becomes kinematically forbidden and the main channels are again $b\bar{b}$ and $\tau\bar{\tau}$.

3.3 Annihilation Through Resonances

One of the new features of the NMSSM is its much richer scalar/pseudo-scalar Higgs sector as compared to the MSSM. Thus, one expects new possibilities for having $\Omega h^2 \approx 0.1$ corresponding to annihilation of the LSP through a Higgs resonance. Starting from a point to the right of the WMAP allowed band in fig. 1 (where the relic density is large) we will now vary the Higgs sector parameters A_λ, A_κ to see whether it is possible to find resonances. A_λ directly determines the heavy Higgs doublet mass m_A , eq. (2.11), whereas A_κ influences the Higgs singlet masses, eq. (2.10). The neutralino sector does not depend on these parameters.

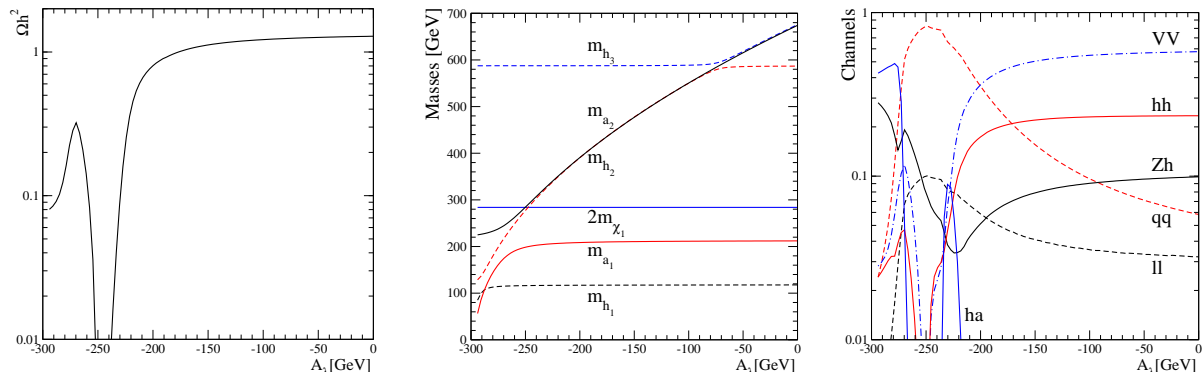


Figure 5: Ωh^2 vs A_λ for $\mu = 300$ GeV, $M_2 = 300$ GeV, $\kappa = 0.1$, $\lambda = 0.1$, $A_\kappa = -50$ GeV and $\tan\beta = 5$. b) Masses of LSP, of scalars (dash) and pseudo-scalars (full) c) Relative contribution of the main annihilation channels.

First, we fix $\lambda = 0.1$, $\kappa = 0.1$, $\mu = M_2 = 300$ GeV and $A_\kappa = -50$ GeV and we vary A_λ . Results for Ωh^2 , the LSP and Higgs masses, as well as the the main channels contributing to the LSP annihilation are displayed in fig 5. For this choice of parameters the LSP mass is $m_{\tilde{\chi}_1^0} = 142$ GeV with a bino fraction of 92%, a higgsino fraction of 7%, and a negligible singlino component. Thus the relic density is rather high, $\Omega h^2 = 1.3$ for $A_\lambda = 0$. The main annihilation channel is into gauge boson pairs. Subdominant channels are into $h_1 h_1$, $Z h_1$ as well as fermion pairs. As A_λ decreases, so does m_A and for $A_\lambda \approx -250$ GeV, the masses of the the heavy scalar and pseudo-scalar Higgs doublets, h_2 and a_2 , are such that $m_{a_2} = m_{h_2} = 2m_{\tilde{\chi}_1^0}$. The relic density then drops sharply. The main decay modes of both a_2 and h_2 being $b\bar{b}$ and $\tau\bar{\tau}$, the dominant LSP annihilation channel near the resonance is into fermion pairs. When $A_\lambda \approx -300$ GeV and one moves away from the s-channel resonance, the LSP still annihilates efficiently into $h_1 a_1$ or $Z h_1$ through a_2 exchange. The relic density again falls into the WMAP allowed range. However, in this region h_1 is excluded by LEP.

Next, we fix $A_\lambda = 0$ and vary A_κ , keeping all the other parameters as above. Results for Ωh^2 , the LSP and Higgs masses, as well as the the main annihilation channels are displayed in fig 6. Note however that the A_λ range in fig 6c is not the same as in fig 6a-b. The

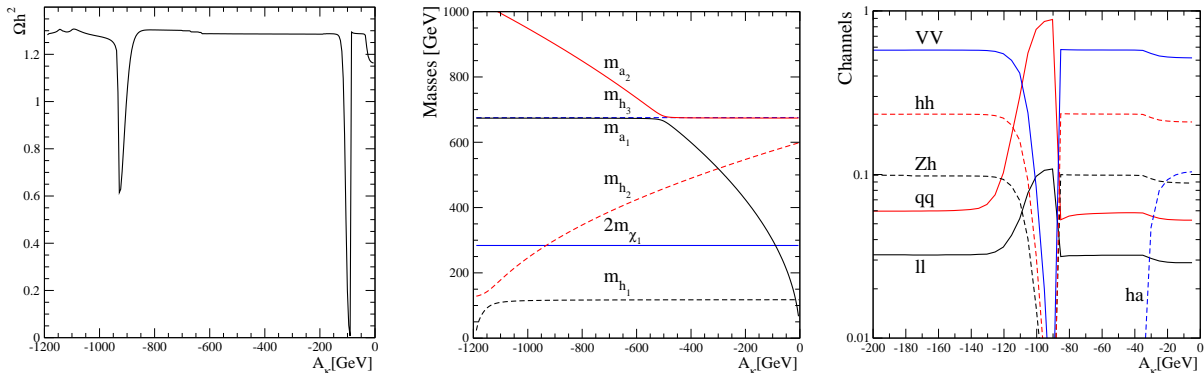


Figure 6: Ωh^2 vs A_κ for $\mu = 300$ GeV, $M_2 = 300$ GeV, $\kappa = 0.1$, $\lambda = 0.1$, $A_\lambda = 0$ and $\tan\beta = 5$. b) Masses of LSP, of scalars (dash) and pseudo-scalars (full) c) Relative contribution of the main annihilation channels.

LSP has the same characteristics as in the previous case. For $A_\kappa \approx -950$ GeV, the scalar (singlet) h_2 is such that $m_{h_2} = 2m_{\tilde{\chi}_1^0}$, and for $A_\kappa \approx -90$ GeV, the pseudo-scalar (singlet) a_1 is such that $m_{a_1} = 2m_{\tilde{\chi}_1^0}$. Far from these resonances, Ωh^2 is large and the preferred annihilation channel is into W pairs. The h_2 resonance is associated with an increase in the annihilation channel $\tilde{\chi}_1^0 \tilde{\chi}_1^0 \rightarrow h_1 h_1$. However LSP annihilation through this resonance is not efficient enough to bring the relic density within the WMAP range. This is because the coupling $\tilde{\chi}_1^0 \tilde{\chi}_1^0 h_2$, eq. (2.17), is suppressed for a bino LSP and a singlet Higgs. Near the a_1 resonance, the pseudo-scalar annihilates mainly into $b\bar{b}$ as shown in fig. 6c. Although the $\tilde{\chi}_1^0 \tilde{\chi}_1^0 h_2$ coupling, eq. (2.18), is also suppressed, annihilation is more efficient through a_1 than through h_2 because of the p-wave suppression factor for a scalar exchange.

3.4 Mixed bino/higgsino: $\mu \approx M_2$ in the NMSSM

We now consider in more details the mixed bino/higgsino case with $\mu = 220$ GeV, $M_2 = 320$ GeV, $\tan\beta = 5$, $A_\lambda = 500$ GeV and $A_\kappa = 0$ (corresponding to the second WMAP allowed region in fig. 1). In fig. 7 we plot the Ωh^2 dependence on the specific NMSSM parameters λ, κ . Theoretically and experimentally excluded regions are similar to those obtained in fig. 3. In the limit $\lambda \rightarrow 0$, the singlino decouples. According to eq. (2.16), μ being fixed, the singlino mass is proportional to κ/λ . Hence, for small λ and $\kappa/\lambda \gtrsim 1/3$, the singlino is heavy and the LSP is a mixed bino (70%) and higgsino (30%), with a mass $m_{\tilde{\chi}_1^0} = 140$ GeV. Its relic density is within the WMAP bounds, the main annihilation channel being into WW , as explained in section 3.1. Smaller values of κ/λ lead to a singlino LSP whose relic density is very large unless one has recourse to some special annihilation mechanism, as will be explained in section 3.5. In the singlino region, one can already see two clear resonances bringing the relic density down for $\lambda \approx 0.1$ and $\kappa \approx 0.01$. One corresponds to an h_2 resonance and the other to a Z resonance. However, these are located in a region ruled out by Higgs searches at LEP.

At larger values of λ and κ , one can see a third resonance as well as a decrease of the relic density below the WMAP allowed region. To see more precisely what occurs in this

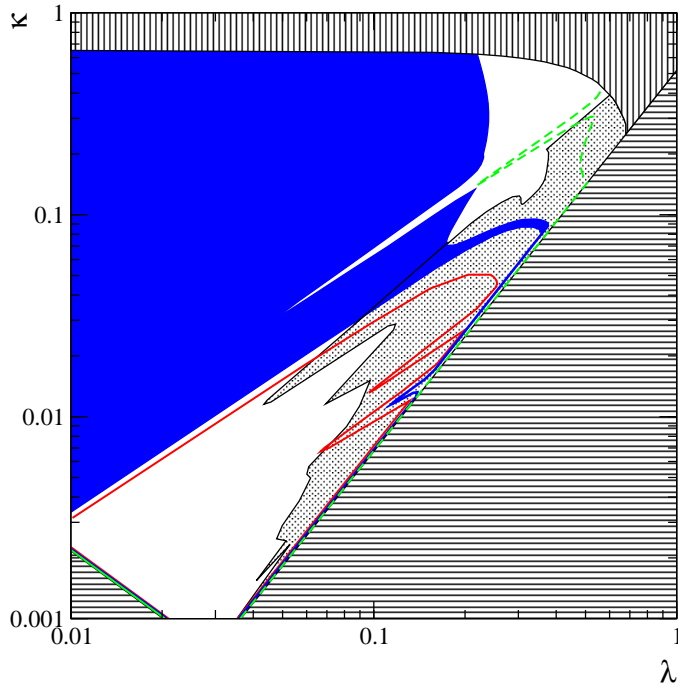


Figure 7: Contour plots for $\Omega h^2 = 0.02$ (dash), $\Omega h^2 = 1$ (full) and region for which $0.0945 < \Omega h^2 < 0.1287$ (blue) in the λ, κ plane for $\mu = 220$ GeV, $M_2 = 320$ GeV, $A_\lambda = 500$ GeV, $A_\kappa = 0$ and $\tan\beta = 5$. Theoretically and experimentally excluded regions are labeled as in fig. 3.

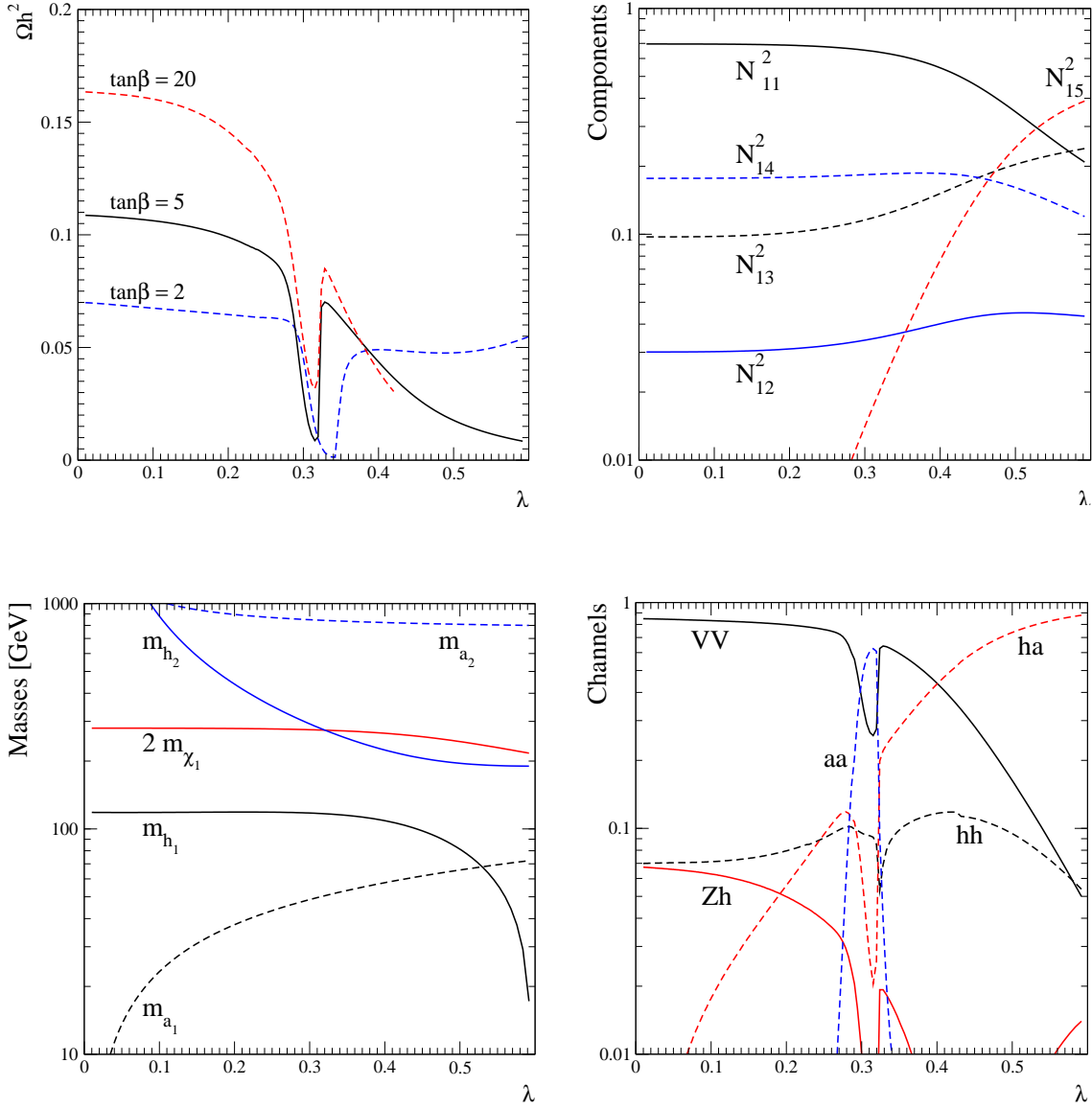


Figure 8: a) Ωh^2 vs λ for $\mu = 220$ GeV, $M_2 = 320$ GeV, $\kappa = 0.2$, $A_\lambda = 500$ GeV, $A_\kappa = 0$ GeV, $\tan\beta = 5$ (full) and $\tan\beta = 2, 20$ (dashed). b) Components of the LSP c) Masses of LSP, of scalars (dash) and of pseudo-scalars (full) d) Relative contribution of main channels for neutralino annihilation.

area of the parameter space, we fix $\kappa = 0.2$ and plot Ωh^2 as a function of λ in fig. 8. We also plot the LSP components, the LSP and Higgs spectrum, and the main annihilation channels. At small values of λ , one can see from fig. 8b that the singlino almost decouples and one recovers the MSSM. The value of Ωh^2 for $\lambda \rightarrow 0$ and $\tan\beta = 5$, fig. 8a, is equal to the MSSM prediction for equivalent parameters. The main annihilation channel, fig. 8d, is WW through Z exchange, with subdominant Zh_1 and h_1h_1 contributions coming from h_1 exchange. As λ increases, the relic density decreases until one encounters the h_2 resonance for $\lambda \approx 0.3$, fig 8c. The relic density then drops and the main annihilation channels reflect the h_2 decay modes, with a dominant a_1a_1 final state. Above the resonance, Ωh^2 keeps decreasing as the LSP becomes dominantly singlino. Recall that for μ and κ fixed, the singlino diagonal mass term, eq. (2.14) goes like $1/\lambda$ while the singlino mixings are proportional to λ . This result for the relic density is counter-intuitive, since for a singlino LSP, annihilation should be suppressed and relic density large. The main annihilation channel in this case is h_1a_1 through t-channel $\tilde{\chi}_1^0$ exchange. The decrease of Ωh^2 with λ can then be understood by an increase of the $\tilde{\chi}_1^0\tilde{\chi}_1^0h_1$ and $\tilde{\chi}_1^0\tilde{\chi}_1^0a_1$ couplings as given in eqs. (2.17,2.18) for a singlino LSP. However, this area of the parameter space is excluded by Higgs searches at LEP, as shown in fig. 7. We will investigate in section 3.5 whether it is possible to find regions in the parameter space with a singlino LSP allowed both by LEP and WMAP constraints.

A similar dependence of Ωh^2 on λ is observed for different values of $\tan\beta$, in fig. 8a. The mass of the LSP varies with $\tan\beta$, so the value of λ for which resonant annihilation occurs is shifted. As we have discussed in section 3.1, when the main annihilation channel is into gauge boson pairs, annihilation is more efficient at low values of $\tan\beta$ where the LSP is less bino-like. For $\tan\beta = 2$ however, no decrease of Ωh^2 occurs at large values of λ . This is due to the fact that both the $\tilde{\chi}_1^0\tilde{\chi}_1^0a_1$ and $\tilde{\chi}_1^0\tilde{\chi}_1^0h_1$ couplings are much weaker for low values of $\tan\beta$.

3.5 Singlino LSP

We explore now scenarios satisfying both LEP and WMAP constraints with a predominantly singlino LSP. For this we scanned over the whole parameter space of the NMSSM in the range $\lambda < 0.75$, $\kappa < 0.65$, $2 < \tan\beta < 10$, $100 < \mu < 500$ GeV, $100 < M_2 < 1000$ GeV, $0 < A_\lambda < 1000$ GeV and $0 < -A_\kappa < 500$ GeV. We found three classes of models: a mixed singlino/higgsino LSP that annihilates mainly into h_1a_1 and VV , an almost pure singlino that annihilates through a Z or Higgs resonance and a singlino where dominant channels are coannihilation ones. In table 2 we show a selection of benchmark points along these lines.

The first scenario is one for which $\mu \ll M_2$ and the LSP is a mixed higgsino/singlino. We give two different examples in table 2. For point 1, the LSP is 88% singlino and 12% higgsino, with a mass of 122 GeV. The main annihilation mode is h_1a_1 through t-channel $\tilde{\chi}_1^0$ exchange, h_1 and a_1 being both mainly singlet (88% and 99% respectively). As we have seen in section 3.4 this is due to the enhanced couplings $\tilde{\chi}_1^0\tilde{\chi}_1^0a_1(h_1)$ for large values of λ . The annihilation into h_1a_1 being too efficient for large values of $\tan\beta$, we chose $\tan\beta = 2$ for this point. Annihilation of the higgsino component into W pairs accounts for the subdominant channel. For point 2, the LSP mass is 148 GeV and the main annihilation channel is WW , which necessitates some sizeable higgsino component (29% here). The subdominant channel h_1a_1 implies the singlino component of the LSP (69%). The singlino fraction cannot be maximal here since there are no important annihilation channels for a pure singlino when λ

Point	1	2	3	4	5	6
λ	0.6	0.24	0.4	0.23	0.31	0.0348
κ	0.12	0.096	0.028	0.0037	0.006	0.0124
$\tan\beta$	2	5	3	3.1	2.7	5
μ [GeV]	265	200	180	215	210	285
A_λ [GeV]	550	690	580	725	600	50
A_κ [GeV]	-40	-10	-60	-24	-6	-150
M_2 [GeV]	1000	690	660	200	540	470
$m_{\tilde{\chi}_1^0}$ [GeV]	122	148	35	10	15	203
$N_{13}^2 + N_{14}^2$	0.12	0.29	0.12	0.03	0.06	0.02
N_{15}^2	0.88	0.69	0.87	0.95	0.94	0.96
$m_{\tilde{\chi}_2^0}$ [GeV]	259	199	169	87	182	214
$m_{\tilde{\chi}_1^\pm}$ [GeV]	258	193	171	139	196	266
m_{h_1} [GeV]	117	116	36	22	34	115
S_{13}^2	0.88	0.04	0.98	1.00	1.00	0.04
m_{h_2} [GeV]	128	158	117	114	113	163
S_{23}^2	0.11	0.96	0.01	0.00	0.00	0.96
m_{a_1} [GeV]	114	59	56	18	15	214
$P_{12}^{\prime 2}$	0.99	1.00	0.99	1.00	0.99	1.00
Ωh^2	0.1092	0.1179	0.1155	0.1068	0.1124	0.1023
Channels	<i>ha</i> (73%) <i>VV</i> (13%) <i>Zh</i> (8%) <i>hh</i> (3%) <i>qq</i> (2%) <i>ll</i> (1%)	<i>VV</i> (75%) <i>ha</i> (17%) <i>hh</i> (5%) <i>Zh</i> (2%)	<i>qq</i> (65%) <i>ll</i> (35%)	<i>qq</i> (93%) <i>ll</i> (7%)	<i>aa</i> (92%) <i>qq</i> (7%) <i>ll</i> (1%)	$\tilde{\chi}_2^0 \tilde{\chi}_2^0 \rightarrow X$ (81%) $\tilde{\chi}_1^0 \tilde{\chi}_2^0 \rightarrow X$ (15%) $\tilde{\chi}_1^0 \tilde{\chi}_1^\pm \rightarrow X$ (2%) <i>qq</i> (2%)

Table 2: Benchmark points with a singlino LSP satisfying both LEP and WMAP constraints

is not so large and the channel $h_1 a_1$ is not dominant.

We give in table 2 the characteristics of three typical scenarios with light singlinos. The only efficient annihilation mode for a very light singlino (below 50 GeV) is via a Z or a Higgs resonance. For point 3, the LSP is 87% singlino with a mass of 35 GeV and annihilates through a Z exchange. In this scenario, although the singlino component dominates, a 12% higgsino component is sufficient to ensure efficient annihilation through the Z . As for the main annihilation channels they are characteristic of the Z decay modes, mainly into quark pairs and lepton pairs. Neutralinos of 30 GeV that satisfy the WMAP upper bound were also found in SUGRA models with non-universal gaugino masses [24]. Because the scalar/pseudo-scalar Higgs states in the NMSSM can be much below the Z mass while passing all the LEP constraints, we expect to find even lighter singlino LSP's in models where $2m_{\tilde{\chi}_1^0} \approx m_h$. We show two examples (point 4 and 5) of such models in table 2. In both cases the LSP annihilates via a light scalar dominantly singlet ($S_{13}^2 \approx 1$). This scalar decays either into $b\bar{b}$ (point 4) or, when kinematically accessible, into $a_1 a_1$ (point 5), the a_1 being also mainly singlet. The Higgs sector of such models is of course severely constrained by LEP, in particular the limit on the SM-like scalar, here the second scalar, h_2 . For this reason most scenarios with light singlinos have $\tan\beta \approx 3$ which is the value for which the lightest visible (*ie* non singlet) Higgs mass, m_{h_2} , is maximized [11]. Note that a light singlino requires $\kappa \ll \lambda$ and not too large value for μ . The singlino masses for point 4 and 5 are respectively 10 GeV and 15 GeV. We found points in the parameter space with singlinos as light as a few GeV.

For $\kappa \lesssim \lambda \ll 1$, the LSP is heavy with a large singlino component. No efficient annihilation mechanism is then available. However coannihilation with heavier neutralinos and charginos can be very efficient especially for a higgsino-like NLSP. Point 6 in table 2 gives an example of such a scenario. The LSP is 96% singlino with a mass of 204 GeV. The mass difference with the NLSP $\tilde{\chi}_2^0$ is 11 GeV. The coannihilation channels are overwhelmingly dominant. The $\tilde{\chi}_2^0$ higgsino component is just enough (28%) for efficient annihilation. The main channels are $\tilde{\chi}_2^0 \tilde{\chi}_2^0 (\tilde{\chi}_1^0) \rightarrow t\bar{t}, b\bar{b}$ and correspond to annihilation through h_3 and a_2 exchange. For this point, h_3 and a_2 belong to the heavy Higgs doublet with $m_A \approx 470$ GeV, so that we are close to a (double) resonance. Such a resonance is not necessary though, in order to have efficient $\tilde{\chi}_2^0$ annihilation. We also found points in the parameter space with a heavy singlino where the dominant channel was $\tilde{\chi}_2^0 \tilde{\chi}_2^0 (\tilde{\chi}_1^0) \rightarrow VV$ through Z exchange.

4 Conclusions

In the NMSSM, the same mechanisms as for the MSSM are at work for neutralino annihilation: into fermion pairs through s-channel exchange of a Z or Higgs, into gauge boson pairs through either Z/h s-channel exchange or t-channel exchange of heavier neutralinos or charginos. The new feature of the NMSSM is the presence of additional Higgs states, which means additional regions of parameter space where rapid annihilation through a s-channel resonance can take place. We found that annihilation through a Higgs resonance is dominant in large regions of the parameter space and this even at low to intermediate values of $\tan\beta$. Furthermore, new channels also open up since light Higgs state can be present. For example annihilation channels into Zh, hh, ha or even aa can contribute significantly to the relic density. These proceed through s-channel $Z/h/a$ exchange or t-channel neutralino

exchange. Despite the additional annihilation channel available because of a richer Higgs sector, annihilation of neutralinos is not always favoured in the NMSSM. In general the singlino component of the LSP tends to reduce the annihilation cross-section. Therefore one expects that the relic density of dark matter strongly constrain models with a large singlino component. We found however regions of the parameter space where a singlino LSP gives the right amount of dark matter, either for large λ , s-channel resonances into a Z or a Higgs, or coannihilation with $\tilde{\chi}_2^0, \tilde{\chi}_1^\pm$.

For a bino LSP, compatibility with the WMAP result can be recovered in the NMSSM. This however requires tuning the parameters of the model such that $2m_{\tilde{\chi}_1^0}$ is only a few GeV below the mass of a Higgs boson. In models where $M_2 = 2M_1$ as we have discussed here, this would also mean that one has a chargino mostly wino with a mass $m_{\tilde{\chi}_1^\pm} \approx 2m_{\tilde{\chi}_1^0} \approx m_{h_1}$. Such a degeneracy between the chargino mass and the Higgs mass could be measured at the ILC. If the Higgs boson is mostly doublet, it might be hard to disentangle the NMSSM from the MSSM. If it is singlet, mass relation between the NMSSM Higgs states would be different from what expected in the MSSM. A mostly singlet Higgs state could eventually be observable at the LHC with high luminosity [25].

In the case of a mixed bino/higgsino LSP, annihilation relies, as in the MSSM, on s-channel Z exchange and t-channel neutralino/chargino exchange. If the singlino state is not heavy and decouples, *ie* λ not too small and κ not too large, the five neutralino states might be visible at the LHC/ILC. This would be a clear signature of the NMSSM.

Finally, in the singlino LSP case, μ cannot be too large. One therefore would expect visible higgsinos at the LHC. The singlino LSP would however appear at the end of the decay chain in any sparticle pair production process, which might complicate the detection task as it was the case at LEP [13].

As a concluding remark, one should mention that, if one assumes minimal flavour structure, $b \rightarrow s\gamma$ might impose strong constraints on the NMSSM parameter space, especially for large values of λ where the charged Higgs mass, eq. (2.9), could be lighter than in the MSSM. A complete study of the constraints coming from flavour physics should be the next step of the phenomenological study of the NMSSM.

Acknowledgements

This work was supported in part by GDRI-ACPP of CNRS and by grants from the Russian Federal Agency for Science, NS-1685.2003.2 and RFBR 04-02-17448. The manuscript was finished in Les Houches, Physics at TeV Colliders 2005.

References

- [1] C. L. Bennett *et al.*, *Astrophys. J. Suppl.* **148** (2003) 1 [arXiv:astro-ph/0302207];
D. N. Spergel *et al.*, *Astrophys. J. Suppl.* **148** (2003) 175 [arXiv:astro-ph/0302209].
- [2] G. Bélanger, F. Boudjema, A. Pukhov and A. Semenov, *Comput. Phys. Commun.* **149** (2002) 103, [arXiv:hep-ph/0112278];
G. Bélanger, F. Boudjema, A. Pukhov and A. Semenov, arXiv:hep-ph/0405253.
- [3] J. R. Ellis, K. A. Olive, Y. Santoso and V. C. Spanos, *Phys. Lett.* **B565** (2003) 176 [arXiv:hep-ph/0303043];
H. Baer and C. Balazs, *JCAP* **0305** (2003) 006 [arXiv:hep-ph/0303114];
U. Chattopadhyay, A. Corsetti and P. Nath, *Phys. Rev.* **D68** (2003) 035005 [arXiv:hep-ph/0303201];
S. Profumo and C. E. Yaguna, arXiv:hep-ph/0407036;
E. A. Baltz and P. Gondolo, arXiv:hep-ph/0407039;
G. Bélanger, F. Boudjema, A. Cottrant, A. Pukhov and A. Semenov, arXiv:hep-ph/0407218.
- [4] J. E. Kim and H. P. Nilles, *Phys. Lett.* **B138** (1984) 150.
- [5] H. P. Nilles, M. Srednicki and D. Wyler, *Phys. Lett.* **B120** (1983) 346;
J. M. Frere, D. R. T. Jones and S. Raby, *Nucl. Phys.* **B222** (1983) 11;
J. P. Derendinger and C. A. Savoy, *Nucl. Phys.* **B237** (1984) 307.
- [6] M. Bastero-Gil, C. Hugonie, S. F. King, D. P. Roy and S. Vempati, *Phys. Lett.* **B489** (2000) 359 [arXiv:hep-ph/0006198];
R. Dermisek and J. F. Gunion, arXiv:hep-ph/0502105.
- [7] S. A. Abel, S. Sarkar and P. L. White, *Nucl. Phys.* **B454** (1995) 663 [arXiv:hep-ph/9506359].
- [8] S. A. Abel, *Nucl. Phys.* **B480** (1996) 55 [arXiv:hep-ph/9609323];
C. Panagiotakopoulos and K. Tamvakis, *Phys. Lett.* **B446** (1999) 224 [arXiv:hep-ph/9809475].
- [9] H. P. Nilles, M. Srednicki and D. Wyler, *Phys. Lett.* **B124** (1983) 337;
U. Ellwanger, *Phys. Lett.* **B133** (1983) 187;
J. Bagger and E. Poppitz, *Phys. Rev. Lett.* **71** (1993) 2380 [arXiv:hep-ph/9307317];
J. Bagger, E. Poppitz and L. Randall, *Nucl. Phys.* **B455** (1995) 59 [arXiv:hep-ph/9505244].
- [10] J. R. Ellis, J. F. Gunion, H. E. Haber, L. Roszkowski and F. Zwirner, *Phys. Rev.* **D39** (1989) 844;
M. Drees, *Int. J. Mod. Phys.* **A4** (1989) 3635;
U. Ellwanger, M. Rausch de Traubenberg and C. A. Savoy, *Phys. Lett.* **B315** (1993) 331 [arXiv:hep-ph/9307322];
Nucl. Phys. **B492** (1997) 21 [arXiv:hep-ph/9611251];
S. F. King and P. L. White, *Phys. Rev.* **D52** (1995) 4183 [arXiv:hep-ph/9505326].

- [11] U. Ellwanger, *Phys. Lett.* **B303** (1993) 271 [hep-ph/9302224];
T. Elliott, S. F. King, P. L. White, *Phys. Lett.* **B305** (1993) 71 [hep-ph/9302202],
Phys. Lett. **B314** (1993) 56 [hep-ph/9305282], *Phys. Rev.* **D49** (1994) 2435 [hep-ph/9308309];
P. Pandita, *Phys. Lett.* **B318** (1993) 338, *Z. Phys.* **C59** (1993) 575;
S. Ham, S. Oh, B. Kim, *J. Phys.* **G22** (1996) 1575 [hep-ph/9604243];
U. Ellwanger and C. Hugonie, *Eur. Phys. J.* **C25** (2002) 297 [arXiv:hep-ph/9909260];
U. Ellwanger and C. Hugonie, arXiv:hep-ph/0504269.
- [12] U. Ellwanger, J. F. Gunion and C. Hugonie, arXiv:hep-ph/0503203.
- [13] U. Ellwanger and C. Hugonie, *Eur. Phys. J.* **C5** (1998) 723 [arXiv:hep-ph/9712300];
U. Ellwanger and C. Hugonie, *Eur. Phys. J.* **C13** (2000) 681 [arXiv:hep-ph/9812427].
- [14] B. R. Greene and P. J. Miron, *Phys. Lett.* **B168** (1986) 226;
R. Flores, K. A. Olive and D. Thomas, *Phys. Lett.* **B245** (1990) 509;
K. A. Olive and D. Thomas, *Nucl. Phys.* **B355** (1991) 192;
S. A. Abel, S. Sarkar and I. B. Whittingham, *Nucl. Phys.* **B392** (1993) 83 [arXiv:hep-ph/9209292];
A. Stephan, *Phys. Lett.* **B411** (1997) 97 [arXiv:hep-ph/9704232]; *Phys. Rev.* **D58** (1998) 035011 [arXiv:hep-ph/9709262];
A. Menon, D. E. Morrissey and C. E. M. Wagner, *Phys. Rev.* **D70** (2004) 035005 [arXiv:hep-ph/0404184].
- [15] D. G. Cerdeno, C. Hugonie, D. E. Lopez-Fogliani, C. Munoz and A. M. Teixeira, *JHEP* **0412** (2004) 048 [arXiv:hep-ph/0408102].
- [16] U. Ellwanger, J. F. Gunion and C. Hugonie, *JHEP* **0502** (2005) 066 [arXiv:hep-ph/0406215].
- [17] A. Pukhov *et al.*, [arXiv:hep-ph/9908288];
E. Boos *et al.* [CompHEP Collaboration], *Nucl. Instrum. Meth.* **A534** (2004) 250 [arXiv:hep-ph/0403113];
A. Pukhov, [arXiv:hep-ph/0412191].
- [18] A. Semenov, in preparation.
- [19] A. Semenov, *Comput. Phys. Commun.* **115** (1998) 124;
A. Semenov, arXiv:hep-ph/0208011.
- [20] A. Semenov, *Nucl. Instrum. Meth.* **A502** (2003) 558 [arXiv:hep-ph/0205020].
- [21] F. Boudjema and A. Semenov, *Phys. Rev.* **D66** (2002) 095007 [arXiv:hep-ph/0201219].
- [22] B. C. Allanach, G. Belanger, F. Boudjema and A. Pukhov, *JHEP* **0412**, (2004) 020 [arXiv:hep-ph/0410091].
- [23] G. Belanger, S. Kraml and A. Pukhov, arXiv:hep-ph/0502079.

- [24] G. Belanger, F. Boudjema, A. Cottrant, A. Pukhov and S. Rosier-Lees, *JHEP* **0403** (2004) 012 [arXiv:hep-ph/0310037];
A. Bottino, F. Donato, N. Fornengo and S. Scopel, *Phys. Rev.* **D68**, 043506 (2003) [arXiv:hep-ph/0304080].
- [25] C. Hugonie and S. Moretti, *Proc. of the APS/DPF/DPB Summer Study on the Future of Particle Physics (Snowmass 2001)*, eConf **C010630** (2001) P108 [arXiv:hep-ph/0110241].